Effects of oxygen and water vapour on adhesion of scale grown on ferritic stainless steels in solid oxide fuel cells

Thanasak Nilsonthi*

High Temperature Corrosion Research Centre and Department of Materials and Production Technology Engineering, Faculty of Engineering, King Mongkut's University of Technology North Bangkok, 1518, Pracharat 1 Road, Wongsawang, Bangsue, Bangkok, 10800, Thailand

Abstract. The adhesion of thermal oxide scale grown at 800°C on ferritic stainless steel AISI 441 proposed as SOFCs interconnectors was investigated. The influence of oxidising atmosphere was considered by 20% O_2-N_2 or 20% H_2O-N_2 as the representative cathode and anode atmospheres, respectively. A tensile test in an SEM chamber was used to assess the adhesion behaviour. The spallation of oxide scale on AISI 441 has to important as the candidate of interconnectors in SOFCs. The adhesion energy was considered as strain energy stored in the oxide, which was calculated at the first spallation of scale. The adhesion energy of scale on steel substrate was shown in the range of 173-214 J m^{-2}. The adhesion energy of scale on steel oxidised in water vapour was higher than that in oxygen. This might be due to the presence of a silica layer at the scale-steel interface of steel oxidised in water vapour. The qualitative assessment of scale adhesion in terms of strain initiating the first spallation suggested the good adhesion behaviour of scale grown in the anode atmosphere.

Keyword. SOFC interconnectors, Stainless steel, Oxide scale, Adhesion, Water vapour, Oxygen

1 Introduction

Among the types of fuel cells that are currently under development: proton-exchange membrane fuel cells (PEMFCs), phosphoric acid fuel cells (PAFCs), molten carbonate fuel cells (MCFCs), alkaline fuel cells (AFCs), and solid oxide fuel cells (SOFCs). The SOFCs are gaining increased attention. SOFCs have several advantages over other types of fuel cells due to their high operating temperature (600-1000°C) and solid materials. Since they are operated at high temperatures, the SOFCs have a better ability to tolerate the presence of impurities. Also the component is solid, there is no need for electrolyte loss maintenance and electrode corrosion is eliminated [1]. Solid oxide fuel cells are electrochemical conversion device that generates energy by oxidising a fuel. Solid oxide fuel cells use a solid oxide material as the electrolyte.

A solid oxide electrolyte is used in SOFCs to transfer negative oxygen ions from the cathode to the anode. When multiple cells are stacked in a series, an interconnector is used to connect the fuel-side anode and the air-side cathode. It also enables electron transmission from one cell to the next and the external circuit. Ceramic materials, such as doped lanthanum chromite have been proposed as interconnectors for standard SOFCs operating at approximately 1000°C [2-4]. The interconnector must be extremely stable because it is exposed to both the oxidising and reducing sides of the cell at high temperature. As interconnect materials, ceramics have shown to be more effective than metals. However, when compared to metals, these ceramic interconnect materials are quite expensive. As lower temperature (600-800°C) SOFCs are developed, steel-based alloys are becoming more promising. Stainless steels are considered promising interconnector materials [5-8]. Mostly because of their gas-tightness and high electrical conductivity.

In comparison to ceramic materials, economic advantages such as low cost, availability, and processability are also important. Ferritic materials are chosen from among the numerous varieties of stainless steel due to their low coefficient of thermal expansion. However, when stainless steel is used at SOFCs temperatures such as 800°C the oxide scale forms as chromia on the steel substrate [9-11]. This scale is semi-conductor and reduces the electrical conductivity [12, 13]. At high temperatures, the increasing oxide scale can cause spallation resulting in an air gap between the substrate and the oxide, which perform as an insulator [14]. This work has been interested in industrial ferritic grade (AISI 441). This steel has 18% Cr content and is suitable for usage in high temperature applications. Good adhesion is critical to avoid oxide-steel decohesion, which could operate as a local infinite electrical resistor inhibiting current flow through the cell. The scale formation and adhesion on metallic substrates are influenced not only by the metal chemical compositions [15, 16], but also by their roughness and polishing direction. The adhesion of oxide scale on metallic alloys is normally determined by observing the oxide-steel interface qualitatively or directly measuring spallation in service. Only a few testing methods, such as the indentation test [17], have been developed to quantify the interfacial fracture of scale, although they are not entirely precise. Alternatively, the inverted blister test [18, 19] can

* Corresponding author: thanasak.n@eng.kmutnb.ac.th

be used although thin metal specimens are required. The tensile test is also developed to assess scale adherence on stainless steel [20-22]. For this study, the *in situ* tensile tests are employed to measure scale adhesion on a steel substrate. This test allows for continuous observation of oxide scale spallation, while increasing applied strain. The formation of oxide scale on steel isothermally oxidised in 20% O_2-N or 20% H_2O-N_2 as representative cathode and anode atmospheres respectively is investigated. The adhesion of scale in terms of adhesion energy is also studied.

2 Materials and methods

2.1 Materials and oxidation procedures

The study used an AISI 441 sheets of ferritic stainless steel grade, which is available from ARCELOR with a thickness of 2 mm. Table 1 shows the chemical composition of the steel.

Table 1. Chemical composition of the AISI 441 steel (wt.%).

Element	wt.%
Cr	17.83
Ni	0.10
C	0.01
Mn	0.24
Si	0.60
Ti	0.13
Nb	0.55
Fe	Bal.

A sample is cut from AISI 441 sheets and polished with SiC paper up to 1200 grade. Then, the sample is cleaned by an ultrasonic cleaning method using ethanol cleaner, followed by drying in air. The sample is oxidised in a horizontal furnace with 20% O_2-N_2 or 20% H_2O-N_2 as simulated SOFCs atmosphere at 800°C for 100 hours. Oxidation in water vapour (20% H_2O) is calculated by the Clausius-Clapeyron equation as follows,

$$ln\frac{P}{1\ atm} = \frac{-\Delta H^{l\rightarrow v}}{R}\left(\frac{1}{T} - \frac{1}{373}\right) \quad (1)$$

where P is the vapour pressure (0.2 atm), ΔH is the enthalpy change of reaction (40,893 J mol^{-1}), R is the gas constant (8.314 J mol^{-1} K^{-1}), and T is the temperature in Kelvin. Using equation (1), the temperature at 20% of the vapour pressure of water is 332.43 K (59.43°C).

The scale thickness can be calculated by average mass gain as pure chromia assumed. The following equation is commonly used to estimate scale thickness.

$$Scale\ thickness\ (\mu m) = \frac{\Delta m}{A}\cdot\frac{1}{M_O}\cdot M_{FeO}\cdot\frac{1}{\rho_{FeO}}\cdot 10^4 \quad (2)$$

where Δm is the mass change before and after oxidation (g), A is an area (cm^2), M_O is the molecular weight of oxygen (16 g mol^{-1}), M_{FeO} is the molecular weight of iron oxide (72 g mol^{-1}), and ρ_{FeO} is the density of the iron oxide (5.745 g cm^{-3}).

2.2 Determination of oxide scale adhesion energy

The determination of adhesion energy by the tensile test is extensively described in previous papers [20-23]. Electro-erosion is used to prepare specimens with a special shape that fit into the tensile machine sitting in a scanning electron microscope chamber as shown in Figure 1.

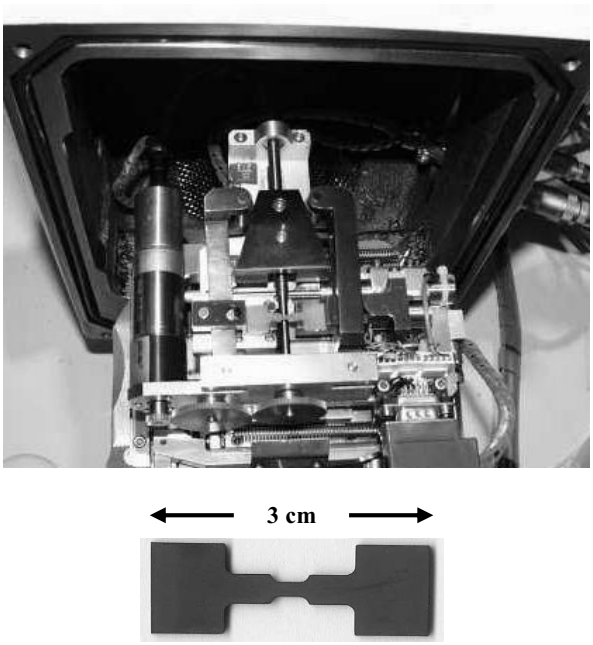

Figure 1. In situ tensile machine and typical shape of steel.

During tensile loading, stress and strain of the sample are continuously recorded. The strain rate is 7×10^{-5} s^{-1} and the test is conducted at room temperature. The scale morphology and scale failure during the tensile test is observed by scanning electron microscope (SEM-EDS, JEOL JSM-6400). The oxide surface is observed by backscatter electrons mode and secondary electrons mode with a magnification of 200×, 500×, 1500×, and 2000×. The adhesion energy of the oxide scale is identified as interfacial fracture energy which is derived from stress and strain at the first spallation. Due to the small size machine and sample, the elongation during the test is far from specimen central. Equation (3) is used to evaluate the actual strain.

$$\varepsilon_{actual} = \varepsilon_{experiment} - \left[\sigma\left(\frac{1}{E_{experiment}} - \frac{1}{E_{metal}}\right)\right] \quad (3)$$

where ε_{actual} is actual metal strain, $\varepsilon_{experiment}$ is an experimental strain of the metal, σ is metal stress (GPa), $E_{experment}$ is experimental Young's modulus of the metal (GPa), and E_{metal} is Young's modulus of the metal (GPa).

The adhesion energy of oxide scale grown on metal have been published [20, 21]. As is widely accepted [24], it is assumed that the scale-metal interface has complete adhesion. The scale-metal interfacial fracture is called as scale spallation. The mechanical adhesion energy at the initial spallation can be determined using the following equation.

$$G = W \cdot \vartheta \quad (4)$$

where G is the mechanical adhesion energy (J m^{-2}), W is the strain energy per unit volume accumulated in the oxide scale until the first spallation (J m^{-3}), and ϑ is the scale thickness (m). The strain energy can be calculated using the stress-strain curve in loading and transverse directions until the first spallation. The strain energy is calculated by the following equation as described in the literature [20, 21].

$$W = \int \sigma \cdot d\varepsilon = \sum W_{fx} + \sum W_{fy} \quad (5)$$

3 Results and discussion

The average mass gain was used to calculate the thickness of the oxide scale, assuming pure chromia formation. The thickness of the oxide scale was 1.67 um for steel oxidised in 20% O_2-N_2, which was higher than 1.09 um for steel oxidised in 20% H_2O-N_2. Scanning electron microscopy was used to examine the surface morphology of steel isothermally oxidised in oxygen and water vapour as shown in Figure 2.

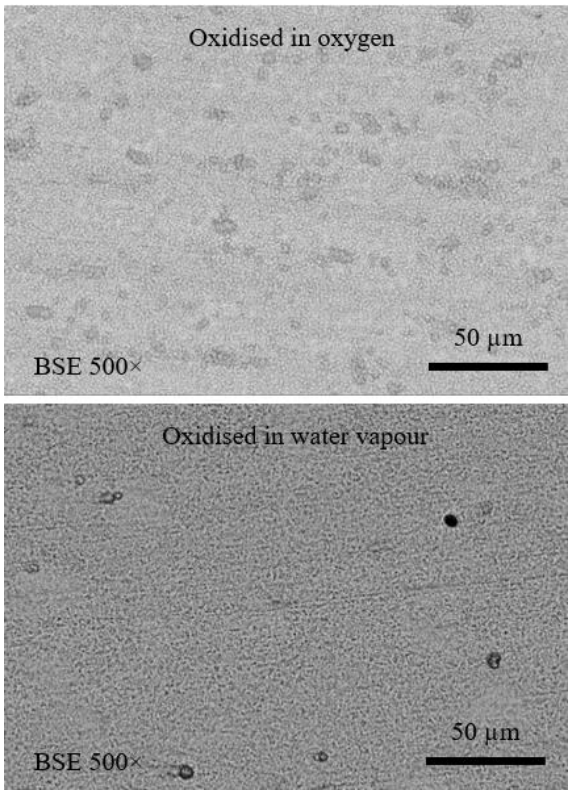

Figure 2. Surface morphology of steel oxidised in oxygen and water vapour.

It was seen that the surface of steel oxidised in water vapour seems to be smoother. Figure 3 illustrates the surface of steel oxidised in oxygen with a magnification of 2000× by secondary electrons mode was shown. An energy-dispersive spectroscopy equipped with a scanning electron microscope was applied to characterise the steel surface. Peaks of Fe, Cr, O, C and Ti were detected. This indicated the existence of oxide containing Cr and Ti at the surface. Meanwhile, Figure 4 illustrates the surface of steel oxidised in water vapour with a magnification of 1500× by secondary electrons mode was shown. Peaks of Fe, Cr, O, C and Ti were observed. The predominance of Cr and Ti was presented on both steels. The scale consisted of major Cr_2O_3-rich oxide and dispersion of TiO_2 as reported [11].

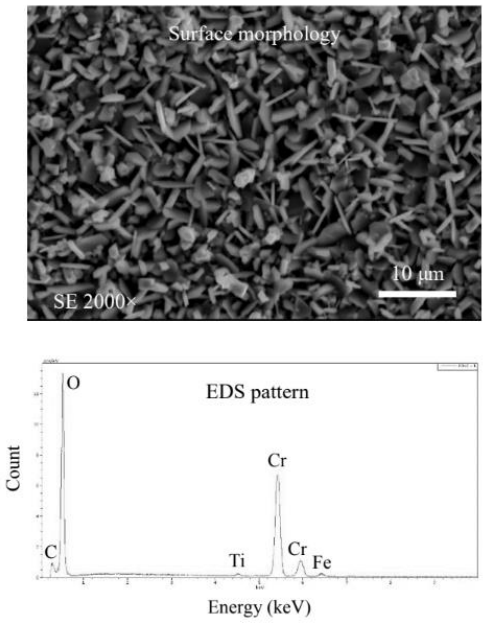

Figure 3. Surface morphology of steel oxidised in oxygen magnified of 2000× and EDS pattern on the surface of steel oxidised in oxygen.

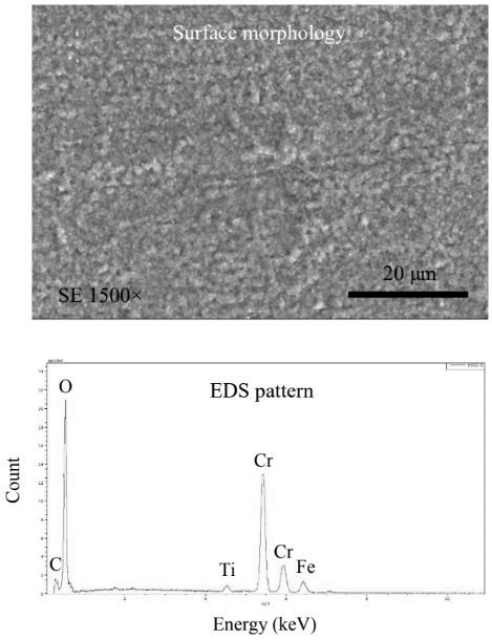

Figure 4. Surface morphology of steel oxidised in water vapour magnified of 1500× and EDS pattern on the surface of steel oxidised in water vapour.

For a tensile test, scale transverse cracks perpendicular to the tensile loading was first observed, followed by local scale spallation. Figure 5 depicts the evolution of scale failure during the tensile test. In these images, steel oxidised in 20% H_2O-N_2 significantly showed less spallation. However, it can be noted that the through-scale transverse cracks perpendicular to the tensile loading was first observed, followed by local scale spallation. This indicated that the steel oxidised in H_2O-N_2 was smoother and less defective. The force of spallation was increased with increasing strain. It should be also noted that the transverse crack on steel oxidised in water vapour was evidently increased by strain. Figure 6 presents the strain initiating the first spallation of the steel oxidised in H_2O-N_2 was 5.50%. This value was higher than that of the steel oxidised in O_2-N_2 which was 2.70%.

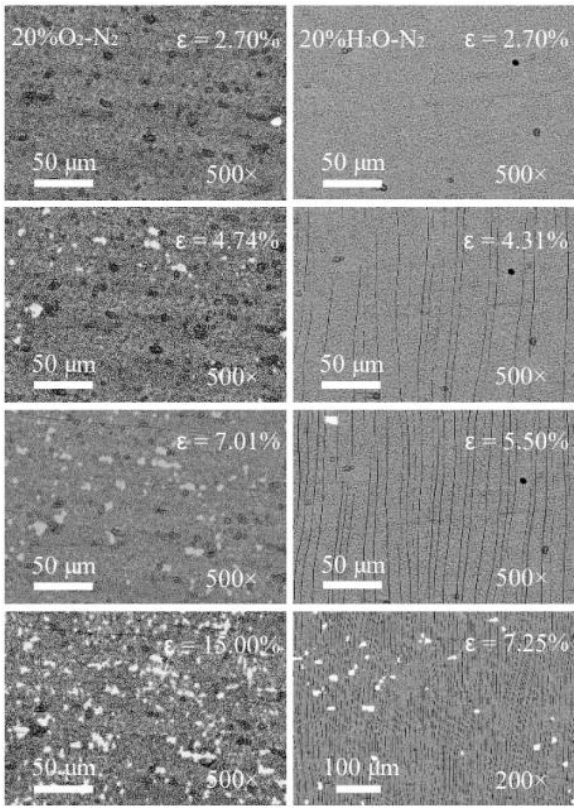

Figure 5. Evolution of scale failure on steel oxidised at 800°C during 100 h in 20%O_2-N_2 (left) and 20%H_2O-N_2 (right).

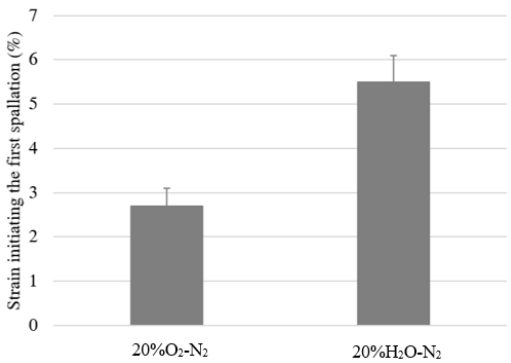

Figure 6. Strain initiating the first spallation of scale on steel oxidised at 800°C during 100 h in 20%O_2-N_2 and in 20%H_2O-N_2.

The fraction of surface area during the tensile test was recorded. The spallation ratio was obtained from these results and plotted in Figure 7. It was observed that the strain at the first strain of steel oxidised in 20% O_2-N_2 was lower than that of the steel oxidised in 20% H_2O-N_2. Moreover, the spallation ratio of steel oxidised in 20% O_2-N_2 was obviously increased with increasing strain. It can be noted that the spallation ratio of steel oxidised in 20% H_2O-N_2 trends to be identical for initiating strain, while rapidly increased with increasing strain for steel oxidised in 20% O_2-N_2.

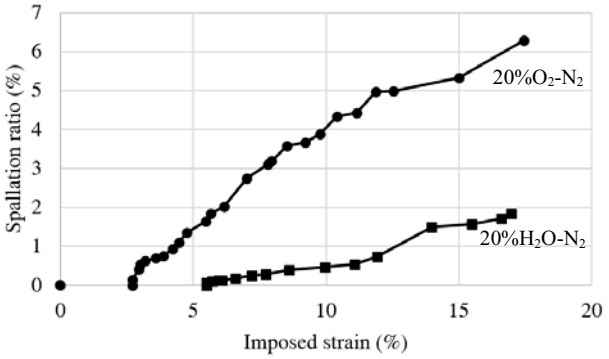

Figure 7. Spallation ratio of oxide scale on steel oxidised at 800°C during 100 h in 20%O_2-N_2 and in 20%H_2O-N_2.

The strain energy was considered as residual stress. Due to the mismatch between the oxide and steel thermal expansion coefficients, it was widely known that oxide growth and cooling on steel accumulates strain in the oxide. The oxide scale was accumulated by residual compressive stress due to oxide growth and cools down with the value of 0.2 GPa. The values of strain energy for chromia scale of 103.47 MJ m^{-3} for steel oxidised in 20% O_2-N_2 and 196.65 MJ m^{-3} for steel oxidised in 20% H_2O-N_2 were shown in Figure 8. It was observed that the strain energy of steel oxidised in 20% H_2O-N_2 was higher than that of the steel oxidised in 20% O_2-N_2.

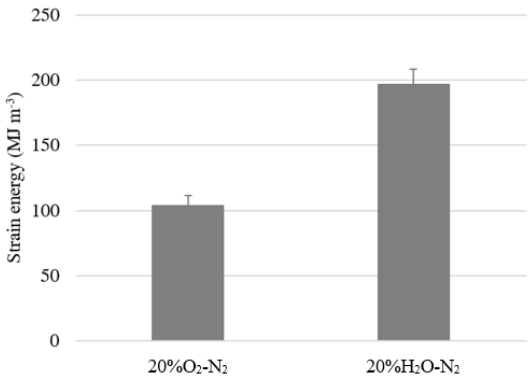

Figure 8. Strain energy of oxide scale formed in 20%O_2-N_2 and 20%H_2O-N_2 at 800°C during 100 h.

The calculated adhesion energy of steel oxidised in 20%O_2-N_2 was 172.79 J m^{-2} which was 2.70% of the strain initiating the first spallation. This value was lower than that of the steel oxidised in 20% H_2O-N_2 which was 214.34 J m^{-2} at 5.50% by strain initiating the first

spallation. The mechanical adhesion energy was shown in Figure 9.

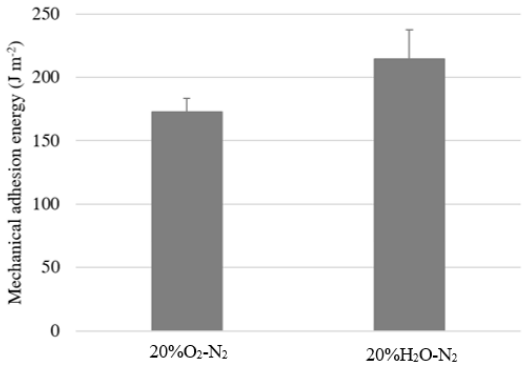

Figure 9. Mechanical adhesion energy of oxide scale formed in 20%O_2-N_2 and 20%H_2O-N_2 at 800°C during 100 h.

Figure 10 and Figure 11 shows tensile specimen in the SEM chamber before and after the tensile loading of steel oxidised at 800°C for 100 hours in 20%O_2-N_2 and 20%H_2O-N_2 respectively. The image was captured using backscatter electrons at a magnification of 30×. It was seen that the spallation of oxide scale revealed global scale failure, particularly on specimen centre. During tensile loading, the maximum stress was subjected in the region of gage length and it was due to the sudden change in the cross-section near the gage length that leads to high stress concentration. The stress greatly affected the global area of the specimen. The scale failure on the specimen was depending on the oxide scale formation. The spallation of scale can be seen more in steel oxidised in oxygen and less in steel oxidised in water vapour. This was due to lower adhesion at the scale-steel interface when the scale oxidised in oxygen.

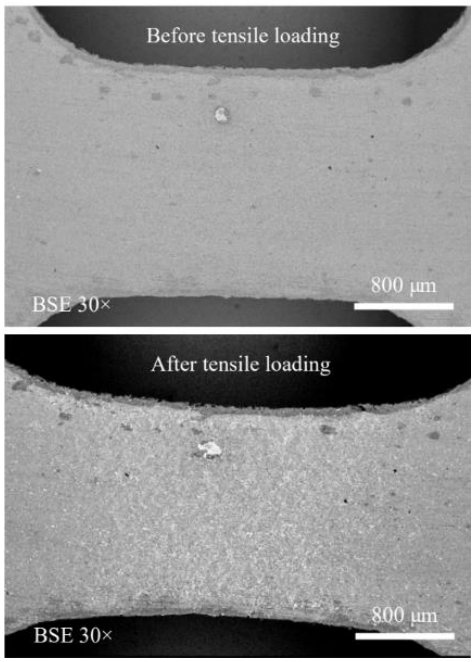

Figure 10. Tensile specimen in SEM chamber before and after tensile loading of steel oxidised in 20%O_2-N_2 at 800°C during 100 h.

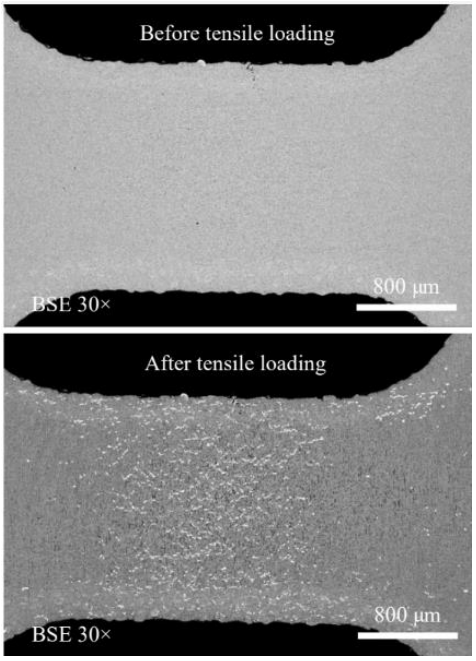

Figure 11. Tensile specimen in SEM chamber before and after tensile loading of steel oxidised in 20%H_2O-N_2 at 800°C during 100 h.

Figure 12 and Figure 13 shows the specimen after the tensile test of steel oxidised at 800°C for 100 hours in 20%O_2-N_2 and 20%H_2O-N_2 respectively. It was shown that the area of scale spalled out after the tensile test. An EDS equipped with SEM was applied to characterise the steel substrate. In the case of steel oxidised in O_2, peaks of Fe, Cr and C were detected. In the case of steel oxidised in H_2O, peaks of Fe, Cr, Si, Ti, C and O were detected.

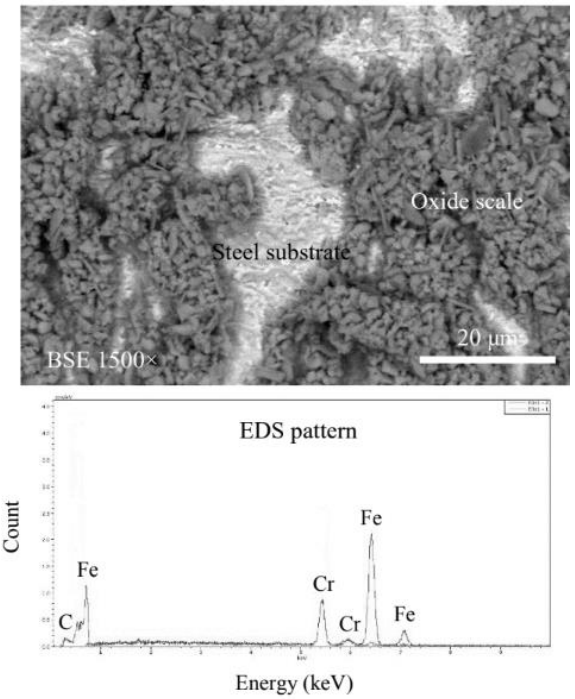

Figure 12. Oxide scale and substrate of steel oxidised in 20%O_2-N_2 at 800°C during 100 h after straining by 27.14% and EDS pattern on metal substrate observed as the white area.

Importantly, this indicated the silica layer formation at the scale-steel interface. This was due to the relatively high Si content (0.60%) in the AISI 441 stainless steel, which corresponded to promoting Si activity in the steel substrate and allowing the formation of an insulating interfacial silica layer. This result was shown to reduce an oxide thickness and exhibited to promote scale adherence. The qualitative assessment of scale adhesion was summarised in Table 2.

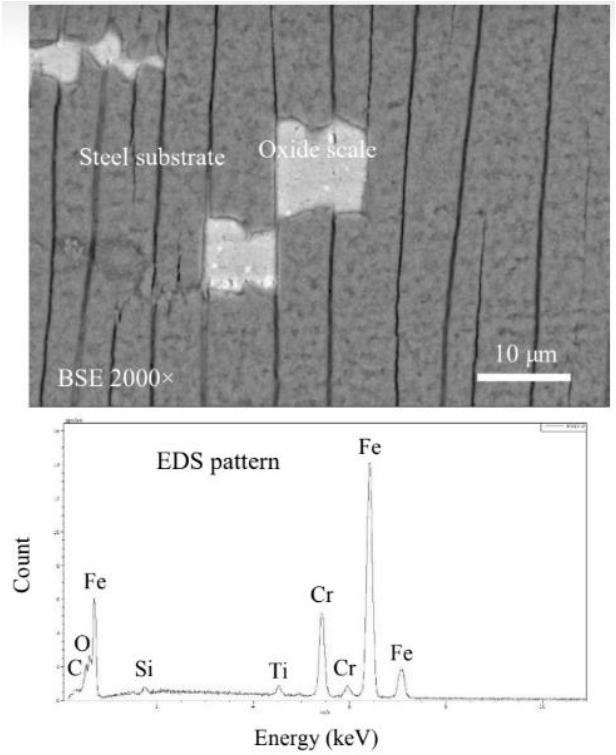

Figure 13. Oxide scale and substrate of steel oxidised in 20%H_2O-N_2 at 800°C during 100 h after straining by 7.65% and EDS pattern on metal substrate observed as the white area.

Table 2. The conclusion of the experiment results.

Scheme	O_2-N_2	H_2O-N_2
Thickness (μm)	1.67	1.09
Strain at first crack (%)	-	3.82
Strain at first spall (%)	2.70	5.50
Strain energy (MJ m^{-3})	103.47	196.65
Adhesion energy (J m^{-2})	172.79	214.34

The qualitative assessment of scale adhesion in terms of strain initiating the first spallation confirmed the good adhesion behaviour of scale grown in water vapour (anode atmosphere). With this value, it was possible to compare results from the literature [25]. It was investigated that the adhesion of thermal oxide scale grown at 800°C in 2% H_2O in H_2 on AISI 441 ferritic stainless steel proposed as interconnectors in solid oxide fuel cells. The adhesion energies were shown to lie in the range 10-100 J m^{-2}. Adhesion values exhibited decreasing with increasing oxide thickness and good adhesion of oxide grown in water vapour compared to oxygen.

For this study, the adhesion energy at the strain initiating the first spallation was found in the range 173-214 J m^{-2}. As a matter of discussion, the good adhesion of scale grown in water vapour compared to oxygen. This could be the result of hydrogen-containing species diffusing inwards in the oxide during scale growth, leading to a scale-steel interface of better growth direction. Another idea was that the oxide containing Si observed at the scale-steel interface during steel oxidised in a water vapour atmosphere. This oxide could be promoted scale adhesion on a steel substrate. Another point of interest was the higher scale thickness of steel oxidised in oxygen compared to water vapour. The adhesion of steel oxidised in oxygen should be less. This might be due to forming voids at the scale-steel interface during metals diffuse to the external scale. The thicker scale had higher voids. Then the adhesion should be worse.

The significance of this study was to focus on the adhesion of oxide scale on the ferritic stainless steel AISI 441. Comparison between oxidation in oxygen and water vapour. Because of high-temperature operation, the oxide scale that grows on SOFCs can cause spallation resulting an insulating air gap between the oxide and the substrate. It could inhibit current flow through the cell. Adhesion results should confirm whether the atmosphere could grow oxide scale adhesive proper to be used as SOFCs interconnectors. The materials used as components have thermally challenged that need to be solved. For improving materials as shown in the literature [26], a concentrated solar power plant (CSP) was another future sustainable energy source like fuel cells which produce electrical energy by chemical reactions. The CSP was the most efficient, reliable, and cost-effective. However, the corrosion was still violent for most materials at high temperature, thus the selection of the material was important. The ferritic stainless steel AISI 409 can be improved by the Al slurry coating technique.

4 Conclusion

The ferritic stainless steel AISI 441 on a candidate to be used as interconnectors in SOFCs was isothermally oxidised in oxygen (cathode atmosphere) and water vapour (anode atmosphere). The tensile test was used to determine adhesion energy. From the results, the following conclusions could be drawn:

4.1 The thickness of steel oxidised in 20%H_2O-N_2 was shown more lowly than steel oxidised in 20%O_2-N_2. This might be due to the present silica layer as a barrier at scale-steel interface.

4.2 Tensile loading could be used to assess the adhesion behaviour of oxide formed in the H_2O-N_2 atmosphere, giving through-scale transverse cracking followed by scale spallation, which was unseen when oxidised in O_2-N_2.

4.3 The adhesion energy at the strain initiating the first spallation was found in the range 173-214 J m^{-2}. Adhesion

energy was higher for scale grown in an H_2O-N_2 atmosphere due to the possible formation of an oxide containing Si at the scale-steel interface during scale growth, which promotes scale adhesion.

4.4 Regarding oxidation and oxide scale adhesion, ferritic stainless steel AISI 441 oxidised in water vapour seems to be better than oxidised in an oxygen atmosphere. This was due to lower scale thickness and formation of silica layer on steel oxidised in water vapour.

4.5 The present work studied the oxidation and adhesion of ferritic stainless steel AISI 441. The additional study of ferritic stainless steel AISI 444 should be carried out for comparison.

Acknowledgements

This research was funded by National Science, Research and Innovation Fund (NSRF), and King Mongkut's University of Technology North Bangkok with Contract no. KMUTNB-FF-65-09. Ugine & ALZ (Arcelor-Mittal Group) for the provision of the AISI 441 (F18TNb) stainless steel for the study.

References

1. Fiseha M. Guangul, Girma T. Chala, A comparative study between the seven types of fuel cells, Applied Science and Engineering Progress, 13, 3, (2020): 185-194.
2. W.Z. Zhu, S.C. Deevi, Development of interconnect materials for solid oxide fuel cells, Materials Science and Engineering A, 384, (2003): 227-243
3. C. Déportes, M. Duclot, P. Fabry, J. Fouletier, A. Hammou, M. Kleitz, E. Siebert, J.L. Souquet, *Electrochimie des solides* (Presses Universitaires de Grenoble, France, 1994)
4. L. Antoni, Materials for solid oxide fuel cells: the challenge of their stability, Materials Science Forum, 461-464, (2004): 1073-1090
5. W.J. Quadakkers, J. Piron-Abellan, V. Shemet, L. Singheiser, Metallic interconnectors for solid oxide fuel cells-a review, Materials at High Temperatures, 20, 2 (2003): 115-127
6. Z. Yang, G. Xia, K.D. Meinhardt, K.S. Weil, J.W. Stevenson, Chemical stability of glass seal interfaces in intermediate temperature solid oxide fuel cells, Journal of Materials Engineering and Performance, 13, (2004): 327-334
7. W.Z. Zhu, S.C. Deevi, Development of interconnect materials for solid oxide fuel cells, Materials Science and Engineering A, 384, (2003): 227-243
8. J.W. Fergus, Metallic interconnects for solid oxide fuel cells, Materials Science and Engineering A, 397, (2005): 271-283
9. P. Promdirek, G. Lothongkum, S. Chandra-ambhorn, Y. Wouters, A. Galerie, Materials and Corrosion, 62 (2011): 616-622
10. W. Wongpromrat, H. Thaikan, W. Chandra-ambhorn, S. Chandra-ambhorn, Chromium vaporisation from AISI 441 stainless steel oxidised in humidified oxygen, Oxidation of Metals, 79, 5-6, (2013): 529-540
11. P. Promdirek, G. Lothongkum, S. Chandra-Ambhorn, Y. Wouters, A. Galerie, Oxidation kinetics of AISI 441 ferritic stainless steel at high temperatures in CO_2 atmosphere, Oxidation of Metals, 81, 3-4, (2014): 315-329
12. T. Brylewski, M. Nanko, T. Maruyama, K. Przybylski, Application of Fe–16Cr ferritic alloy to interconnector for a solid oxide fuel cell, Solid State Ionics, 142, (2001): 131-150
13. N. Sakai, T. Horita, Y. P. Xiong, K. Yamaji, H. Kishimoto, M.l E. Brito, H. Yokokawa, T. Maruyama, Structure and transport property of manganese-chromium-iron oxide as a main compound in oxide scales of alloy interconnects for SOFCs, Solid State Ionics, 176 (2005): 681-686
14. S Chandra-Ambhorn, F. Roussel-Dherbey, F. Toscan, Y. Wouters, A. Galerie, Determination of mechanical adhesion energy of thermal oxide scales on AISI 430Ti alloy using tensile test, Materials Science and Technology, 23, 4, (2007): 497-501
15. T. Nilsonthi, S. Chandra-ambhorn, Y. Wouters, A. Galerie, Adhesion of thermal oxide scales on hot-rolled conventional and recycled steels Oxidation of Metals, 79, (2013): 325-335
16. S. Chandra-ambhorn, T. Nilsonthi, Y. Wouters, A. Galerie, Oxidation of simulated recycled steels with 0.23 and 1.03 wt.% Si in Ar–20%H_2O at 900°C, Corrosion Science, 87, (2014): 101-110
17. Q. Ma, J.L. Beuth, F. S. Pettit, G. H. Meier, M.J. Stiger, *Use of Indentation Fracture Tests to Investigate Toughness Loss Mechanisms in Thermal Barrier Coating Systems* (ASM International/TMS, Materials Solutions, Pittsburgh, PA, September, 2005)
18. J. Mougin, M. Dupeux, A. Galerie, L. Antoni, Inverted blister test to measure adhesion energy of thermal oxide scales on metals or alloys, Materials Science and Technology, 18, 10, (2002): 1217-1220
19. J. Mougin, M. Dupeux, L. Antoni, A. Galerie, Adhesion of thermal oxide scales grown on ferritic stainless steels measured using the inverted blister test, Materials Science and Engineering A, 359, (2003): 44-51
20. A. Galerie, F. Toscan, E. N'Dah, K. Przybylski, Y. Wouters, M. Dupeux, Measuring adhesion of Cr_2O_3 and Al_2O_3 scales on Fe-based alloys, Materials Science Forum, 461-464, (2004): 631-638
21. F. Toscan, L. Antoni, Y. Wouters, M. Dupeux, A. Galerie, Oxidation kinetics and scale spallation of iron-chromium alloys with different titanium contents, Materials Science Forum, 461-464, (2004): 705-712
22. S. Chandra-ambhorm, F. Roussel-Dherbey, F. Toscan, Y. Wouters, A. Galerie, M. Dupeux, Determination of mechanical adhesion energy of

thermal oxide scales on AISI 430Ti alloy using tensile test, Materials Science and Technology, 23, 4, (2007): 497-501

23. S. Chandra-ambhorn, T. Nilsonthi, Y. Madi, A. Galerie, Application of the micro-tensile testing to investigate the adhesion of thermal oxide scales grown on AISI 441 stainless steel sheet oxidised in air and water vapour, Key Engineering Materials, 410-411, (2009): 187-193
24. H.E. Evans, Stress effects in high temperature oxidation of metals, International Materials Reviews, 40, 1, (1995): 1-40
25. S. Chandra-Ambhorn, Y. Wouters, L. Antoni, F. Toscan, A. Galerie, Adhesion of oxide scales grown on ferritic stainless steels in solid oxide fuel cells temperature and atmosphere conditions, Journal of Power Sources, 171, (2007): 688-695
26. P. Kongkaoroptham, M. Boonpensin, T. Siripongsakul, P. Promdirek, Corrosion behavior of AISI 409 stainless steel with Al slurry coating in molten salt, Applied Science and Engineering Progress, 15, 1, (2022): 1-7.

* Corresponding author: thanasak.n@eng.kmutnb.ac.th